Short-chain n-alkanes in benthic mats and mosses from the Larsemann Hills, East Antarctica

Chatterjee, Subham; Das, Supriyo Kumar; Behera, Pravat Kumar; Ghosh, Devanita; Chakraborty, Arindam; Patel, Priyank Pravin; Ikehara, Minoru

Citation (APA)

Important note
To cite this publication, please use the final published version (if applicable).
Please check the document version above.

Short-chain *n*-alkanes in benthic mats and mosses from the Larsemann Hills, East Antarctica

Subham Chatterjee [a], Supriyo Kumar Das [a,*], Pravat Kumar Behera [a], Devanita Ghosh [b,c], Arindam Chakraborty [d], Priyank Pravin Patel [e], Minoru Ikehara [f]

[a] *Department of Geology, Presidency University, College Street 86/1, Kolkata 700073, India*
[b] *Centre for Earth Sciences, Indian Institute of Science, Bengaluru 560012, Karnataka, India*
[c] *Civil Engineering and Geosciences, Delft University of Technology, 2628CN Delft, The Netherlands*
[d] *Institute of Earth Sciences, Academia Sinica, Taipei 115, Taiwan, ROC*
[e] *Department of Geography, Presidency University, College Street 86/1, Kolkata 700073, India*
[f] *Centre for Advanced Marine Core Research, Kochi University, Japan*

ARTICLE INFO

ABSTRACT

Variation in leaf colour (green, red and grey) of mosses and lake benthic mats in Antarctica is often linked to water stress and ultraviolet light (UV-B) exposure. Changes in the abundance of organic compounds, such as pectin and phenols, are associated with mechanisms protecting against desiccation and UV radiation. However, the function of *n*-alkanes, especially against UV radiation, is rarely examined. Here, gas chromatography–mass spectrometry and Fourier-transform infrared spectroscopy analyses were performed to study the variation in *n*-alkanes in freshwater lake benthic mats and mosses collected from the Larsemann Hills in East Antarctica. Stable isotopes of organic carbon and nitrogen, environmental DNA characterisation and microscopy-based analyses are used to estimate the presence of cyanobacteria, algae and diatoms in moss and benthic mat consortia. Variation in the short-chain (n-C_{17} to n-C_{20}) versus long-chain (n-C_{21} to n-C_{30}) *n*-alkanes in the mosses and benthic mats with their colour were noted. The research links the relative abundance of short-chain *n*-alkanes to the UV-B exposure and proposes that Antarctic mosses and benthic mats synthesise short-chain *n*-alkanes for protection against UV-B.

1. Introduction

Lake moss and benthic mat consortia thrive on the brink of the physiological limits of life due to the extreme and rapidly changing climate conditions in Antarctica (Sabbe et al., 2004). Benthic mats are found at the bottom and along the fringes of lakes and meltwater ponds. Moss beds, usually fed by meltwater during the austral summer, are mostly confined to moist areas. Green mosses remain close to water bodies and meltwater flow channels, while red, grey and moribund mosses, indicating loss of photosynthetic pigments and water stress, are abundant on the drier and exposed ridges (Robinson et al., 2018). Desiccation is common in dry moss beds.

The green and grey mosses primarily consist of the cosmopolitan species *Bryum pseudotriquetrum*, whereas the moribund mosses consist of both endemic *Schistidium antarctici*, and cosmopolitan *B. pseudotriquetrum* species. The green moss *B. pseudotriquetrum* is primarily observed in moist and shadow zones, whereas grey mosses of the same species are observed in areas receiving direct sunlight. Grey-black moribund moss (*S. antarctici* and *B. pseudotriquetrum*) is mainly found along open and dry meltwater channels. The red colouration of mosses is attributed to the decreased abundance of pectin and phenolic esters in the cell wall and offers increased protection against desiccation (Green et al., 2005; Waterman et al., 2018). A similar variation in pigment colour in Antarctic algae and mosses has been speculated to be an adaptive mechanism to prevent the bleaching of chlorophyll molecules under excessive ultraviolet (UV-B) exposure (Singh et al., 2015).

Stratospheric ozone depletion exposes Antarctic mosses and lake benthic mats to UV-B (280–315 nm) radiation (Robinson and Erickson III, 2015). Antarctic mosses synthesise UV screening compounds (UVSC), such as flavonoids, to withstand elevated levels of UV radiation (Convey and Smith, 2006; Turnbull et al., 2009), and a significantly higher concentration of UVSC is reported in the red mosses (Green et al.,

* Corresponding author.
  E-mail addresses: sdas.geol@presiuniv.ac.in, das.supriyo.kumar@gmail.com (S.K. Das).

2005). The cell wall-bound UVSC is evenly distributed throughout the cell wall of unicellular moss leaves and protects from UV radiation (Clarke and Robinson, 2008). The concentration of the UVSC differs in different moss species (Lovelock and Robinson, 2002). Desiccation concentrates the UVSC and reduces further UV-B damage to dry moribund mosses by shrinking moss cells, although the enzymatic repair is mostly inactive under a desiccated state (Turnbull et al., 2009). This makes dry moribund mosses more tolerant to UV exposure than green ones.

The response of mosses in terms of growth conditions and photosynthetic pigment concentrations to external stresses, such as desiccation, nutrient availability, low temperatures and UV-B exposure, has been studied (Robinson et al., 2000; Wasley et al., 2006). Nonetheless, published studies on *n*-alkane characteristics of Antarctic mosses and benthic mats are rare even though the complete absence of higher vascular plants in Antarctica poses a favourable condition to study the distribution of *n*-alkanes in mosses and lake benthic mats. Studying the adaptive mechanism of primary producers, such as moss and benthic mat, against UV-B is timely, especially when the large year-round tropical ozone hole has become a global concern (Lu, 2022).

Here we report the distribution of *n*-alkanes in green (*B. pseudotriquetrum*), grey (*B. pseudotriquetrum*) and moribund (*B. pseudotriquetrum* and *S. antarctici*) mosses and lake benthic mat consortia, collected from the Larsemann Hills (69°24′S, 76°20′E) in East Antarctica (Fig. 1; Table 1), where a recent increase in the abundance of

moribund mosses has been reported (Robinson et al., 2018). Stable isotopes of organic carbon and nitrogen ($\delta^{13}C$ and $\delta^{15}N$), environmental DNA and microscopy-based analyses were performed to understand the qualitative presence of cyanobacteria, diatoms and green algae in moss and lake benthic mat consortia. Gas chromatography–mass spectrometry (GC–MS) and Fourier transform infrared spectroscopy (FTIR) analyses were used for compound identification. In addition, we observed a variation in *n*-alkane distribution with pigment colour of the mosses and benthic mats and explore a possible connection between the *n*-alkane chain length and UV-B exposure.

2. Site description

The Larsemann Hills (Fig. 1), covering an area of ~50 km², is an ice-free oasis and is the second-largest among the major ice-free oases found along the 5000 km coastline of East Antarctica (Gillieson, 1990). The Larsemann Hills is located between the Vestfold Hills and the Amery Ice Shelf on the south-eastern coast of Prydz Bay in Princess Elizabeth Land in East Antarctica (Hodgson et al., 2005; Chauhan et al., 2015). The Larsemann oasis is one of the warmest areas of East Antarctica, with an average annual temperature of −9.8 °C (Mergelov, 2014). January is the warmest month, with an average temperature of +0.6 °C. The coldest month is August, when temperatures fall to −15.9 °C (Mergelov, 2014). The Larsemann Hills is a comparatively ice-free region consisting of two major peninsulas: Stornes in the west and Broknes in the east, along with
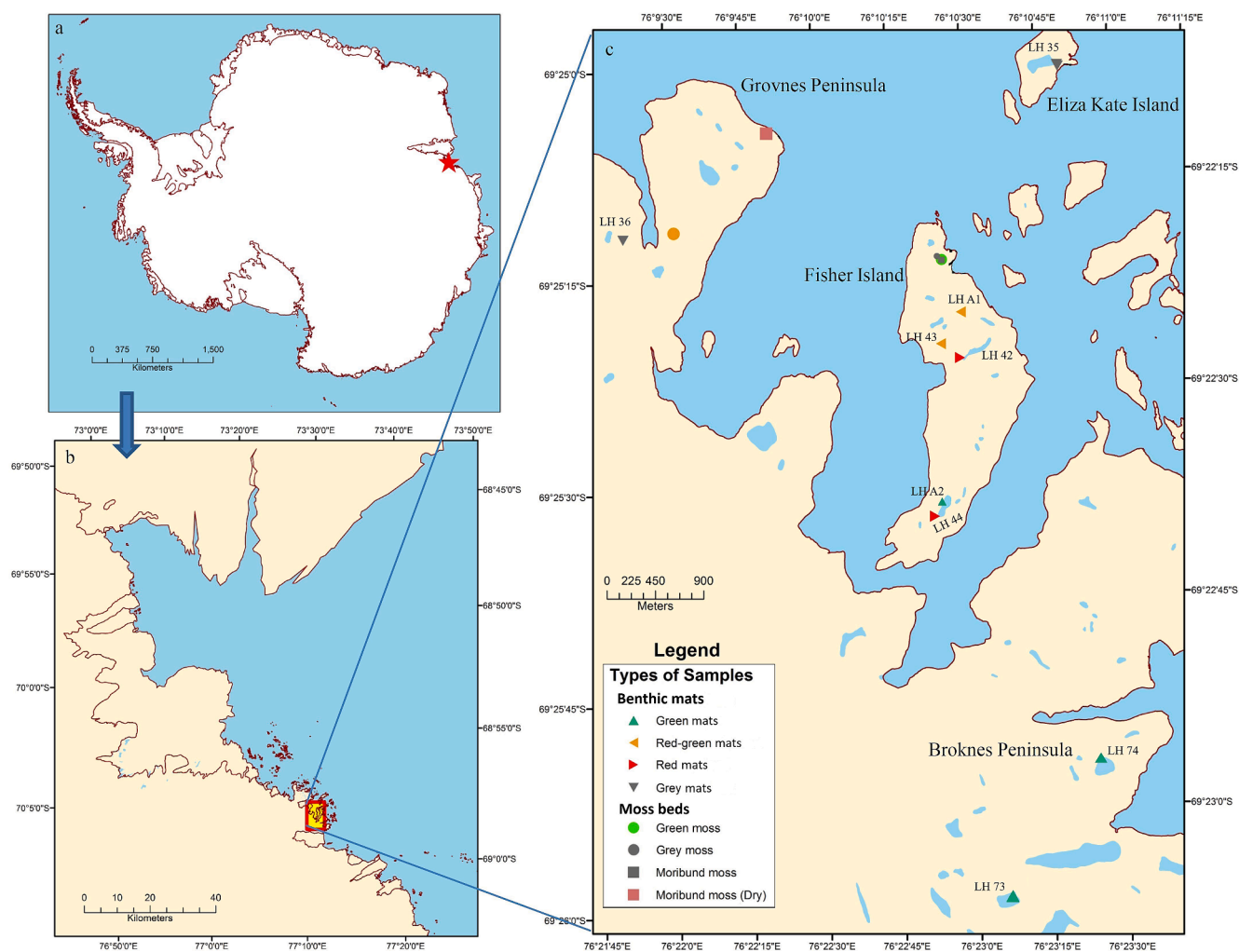
Fig. 1. Sampling locations in Larsemann Hills. The image in the bottom-left shows the sampling area in a red rectangular box. The enlarged form of the rectangular area is shown in the image on the right-hand side. The map shown on the right-hand side shows the different samples collected from Larsemann Hills (shown as a legend within the map). (For interpretation of the references to colour in this figure legend, the reader is referred to the web version of this article.)

Table 1

Sample type and sampling locations of benthic mat and moss samples collected from Larsemann Hills. The altitude of the sampling positions is measured from the mean sea level. The salinity and pH values of lake waters from which benthic mat sampling was performed are also provided.

No	Location	Longitude	Latitude	Altitude (m)	Salinity (ppm)	pH	Sample type
Lake benthic mats							
1	Broknes (LH 73)	76° 22′ 34.7″ E	69° 23′ 56.4″ S	0	63.1	8.9	Green mat
2	Broknes (LH 74)	76° 21′ 01.3″ E	69° 23′ 22.6″ S	0	118	8.9	Green mat
3	Fisher Island (LH A2)	76° 16′ 56.2″ E	69° 23′ 50.7″ S	34	1.2	9.0	Green mat
4	Fisher Island (LH 43)	76° 14′ 45.1″ E	69° 23′ 38.3″ S	33	69.6	8.9	Red-green mat
5	Fisher Island (LH A1)	76° 14′ 22.8″ E	69° 23′30.3″ S	27	534	8.8	Red-green mat
6	Fisher Island (LH 42)	76° 15′ 00.4″ E	69° 23′ 33.7″ S	19	250	9.0	Red mat
7	Fisher Island (LH 44)	76° 17′ 06.1″ E	69° 23′ 52.2″ S	30	171	9.6	Red mat
8	Eliza Kate Island (LH 35)	76° 11′ 18.1″ E	69° 22′ 44.9″ S	19	204	8.7	Grey mat
9	Eliza Kate Island (LH 35)	76° 11′ 18.1″ E	69° 22′ 44.9″ S	19	204	8.7	Grey mat
10	Grovnes (LH 36)	76° 12′ 16.2″ E	69° 25′ 03.2″ S	59	36.5	7.9	Grey mat
Mosses							
11	Fisher Island	76° 13′ 35.8″ E	69° 23′ 32.1″ S	35	–	–	Green moss
12	Fisher Island	76° 13′ 32.1″ E	69° 23′ 33.2″ S	22	–	–	Grey moss
13	Fisher Island	76° 13′ 36.2″ E	69° 23′ 32.2″ S	40	–	–	Moribund moss
14	Grovnes Peninsula	76° 11′ 16.6″ E	69° 24′ 14.0″ S	0	–	–	Moribund moss (dry)

about 130 scattered islands. The Grovnes Peninsula lies between Stornes and Broknes (Fig. 1).

Lakes in the Larsemann Hills remain briefly or partly ice-free during the summer and are covered with thin ice (ca. 2 m) during the rest of the year. Interestingly, the lakes show evidence of higher shorelines in the past but do not exhibit elevated salinity as evidence of evaporation (Roberts and McMinn, 1996; Hodgson et al., 2001). Weak anoxia may persist in the lakes during winter when oxygen is consumed by microorganisms living under the ice (Hodgson et al., 2005).

The region consists of about 150 freshwater lakes of different sizes and depths (Gillieson, 1990), ranging from small shallow ponds (< 1 m depth) to large lakes about 38 m deep. These lakes were either formed in the basins that were exposed when the continental ice cap was retreating (proglacial lakes) or in the basins that were isolated due to isostatic upliftment after the deglaciation event (isolation lakes) (Sabbe et al., 2004). Most lakes are oligotrophic with low concentrations of dissolved nutrients (Ellis-Evans et al., 1998; Sabbe et al., 2004).

3. Materials and methods

3.1. Sampling

Sampling was done between December 2018 and January 2019 (austral summer) during the 38th Indian Scientific Expedition to Antarctica (ISEA). Benthic mats were collected from shallower parts of Lake LH 74 (Discussion Lake) in Broknes Peninsula, lakes LH 42, LH 43, LH 44 and two anonymous lakes (henceforth known as Lake LH A1 and Lake LH A2) in Fisher Island, Lake LH 35 in Eliza Kate Island and Lake LH 36 in Grovnes Peninsula (Fig. 1; Table 1). We observed a change in the colour of the benthic mat consortia collected from the deeper to shallower depths of the lakes. For example, the mats collected from the deeper (~3 m) sections of Lake LH 73 in the Broknes Peninsula are green. In contrast, those collected from the shallower depths (a few cm below water) of the lakes in Fisher Island (Lake LH 42 and Lake LH 44) and Eliza Kate Island (Lake LH 35) are red and grey, respectively (Fig. 1; Table 1). The mat samples from the deeper section of Lake LH 73 were collected using a custom-built Van Veen Grab sampler from a floating platform. The lakes were ice-free during the sampling. Green, grey and moribund mosses were collected from meltwater channels near the lakes in Fisher Island and Grovnes Peninsula (Fig. 1; Table 1). The pH and salinity of the lake waters were measured using a portable Hanna pH Meter. The pH meter was calibrated prior to analysis. The measured pH and salinity values are shown in Table 1. Samples for lipid analysis were stored at −18 °C after collection and freeze-dried. Samples for environmental DNA and microscopic analyses were preserved in 5% ethanol.

3.2. Stable isotope analysis

TOC and total N were measured using an Automated Nitrogen Carbon Analyser - Solids and Liquids (ANCA-SL) elemental analyser (EA). The elemental analyser, coupled to a Europa 20–20 isotope ratio mass spectrometer (IRMS), was used for $\delta^{13}C$ and $\delta^{15}N$ analyses. Prior to the TOC and $\delta^{13}C$ analyses, the samples were acidified with 2 M hydrochloric acid and left overnight to allow inorganic carbon to be liberated as CO_2. The samples were neutralised by repetitively washing with distilled water and subsequently oven-dried at 60 °C in readiness for $\delta^{13}C$ analysis. Results are expressed in the conventional δ notation (‰) using standards calibrated against the international Vienna PeeDee Belemnite (V-PDB) for $\delta^{13}C$ and atmospheric N_2 for $\delta^{15}N$. The results of the $\delta^{13}C$ and $\delta^{15}N$ analyses were calculated as follows:

$$\delta(‰) = \left[\left(R_{sample} / R_{standard} \right) - 1 \right] \times 1000$$

For $\delta^{13}C$ analysis, the R_{sample} and $R_{standard}$ were the $^{13}C/^{12}C$ ratio of the sample and standard, respectively. For $\delta^{15}N$, the R_{sample} and $R_{standard}$ represented the $^{15}N/^{14}N$ ratio of the sample and atmospheric N_2, respectively. Internal standards and blanks were analysed between every eight samples. Duplicate analysis was performed for 20% of the samples.

For carbon isotope analysis, IA-R001 (wheat flour, $\delta^{13}C$ = of −26.43‰) was used as the reference material. Check samples, namely IA-R005 (beet sugar, $\delta^{13}C$ = −26.03‰) and IA-R006 (cane sugar, $\delta^{13}C$ = –11.64‰), were used for quality control. The reference material and check samples were calibrated against the IAEA-CH-6 (sucrose, $\delta^{13}C$ = −10.43‰), distributed by the International Atomic Energy Agency (IAEA) in Vienna.

The IA-R001 (wheat flour; $\delta^{15}N$ = 2.55‰) was used as reference material for $\delta^{15}N$ analysis. Check samples, IA-R001, IA-R045 (ammonium sulphate; $\delta^{15}N$ = −4.71‰), IA-R046 (ammonium sulphate; $\delta^{15}N_{AIR}$ = 22.04‰) and IA-R069 (tuna protein; $\delta^{15}N$ = 11.60‰), were used for quality control. The reference material and check samples were calibrated against an inter-laboratory comparison standard, IAEA-N-1 (ammonium sulphate; $\delta^{15}N$ = 0.4‰), distributed by the IAEA, Vienna. The precision of the analyses (10 replicated standards) was 0.3% for C, 0.03% for N, 0.06‰ for $\delta^{13}C$ and 0.18‰ for $\delta^{15}N$. Duplicate analyses show a reproducibility value of 0.1‰. Stable isotope analyses of the samples were performed at Iso-Analytical Limited in the UK.

3.3. Lipid extraction and analysis

Freeze-dried and homogenised bulk moss and benthic mat samples were extracted with a dichloromethane and methanol mixture (3:1, v/v) using ultrasonication to release lipid biomarkers (Wu et al., 2014). The

combined extract was concentrated using a rotary evaporator under near-vacuum and evaporated to dryness under N_2. The aliphatic hydrocarbon fraction containing *n*-alkanes was separated from the total lipid extracts using silica gel column chromatography and eluted with hexane (Zhang et al., 2004).

The *n*-alkanes were analysed using an Agilent 6890 N gas chromatograph (GC) equipped with a 25 m HP ULTRA 2 fused silica capillary column (i.d. 0.20 mm) and coupled to an Agilent 5973 Network Mass Selective Detector (MSD). The oven temperature was programmed from 50 °C to 120 °C at a rate of 30 °C/min and from 120 °C to 310 °C at a rate of 6 °C/min, followed by an isothermal period of 25 min. Helium was used as a carrier gas. Compound identification was achieved by comparing the GC retention times, fragmentation patterns, and *m/z* peaks of ions and published mass spectra (Fig. 2). Concentrations of alkanes were determined using GC (Agilent 6890 N)-flame ionisation detector (FID) analysis based on peak response. Isoprenoid alkanes were not present in the samples. Lipid extraction was performed at Presidency University in Kolkata. GC–MS analysis was performed at the Centre for Advanced Marine Core Research in Japan.

3.4. Environmental DNA extraction

Environmental DNA can be defined as 'DNA that can be extracted from environmental samples, such as soil, water and air, without first isolating any target organisms' (Taberlet et al., 2012). The set of samples, stored in 5% ethanol, was used to extract the environmental DNA using DNeasy PowerSoil Kit (Qiagen), following the manufacturer's protocol. The isolated environmental DNA was quantified in a Nanodrop 2000 (Thermo Fischer), and the integrity and amplicon sizes were detected by 1% agarose gel electrophoresis.

The bacterial 16S rRNA gene was amplified from the environmental DNA using standard eubacterial primers (amplicon size ~1460 bp; Supplementary Table S1), following the Polymerase Chain Reaction (PCR) protocol given by Ghosh et al. (2014). The amplified and purified PCR products were cloned in *Escherichia coli* strain DH5α using the cloning vector pGEM®-T Easy (Promega). The plasmid DNA with the positive inserts were screened and sequenced using SP6 and T7 primers on ABI Prism 3730 Genetic Analyser with Big Dye Terminator chemistry.

3.5. PCR amplification and Illumina sequencing

The cyanobacteria-specific 16S rRNA gene primers (amplicon size ~680 bp), universal 18S rRNA gene (amplicon size ~600 bp) and *rbcl* gene primers (amplicon size 653–679 bp) (Supplementary Table S1) were used to detect the signatures of cyanobacteria and algal cells in the samples. PCR amplification was made using the isolated environmental DNA as a template. The PCR reaction conditions were used following the referred literature (Supplementary Table S1).

Environmental DNA was extracted using the XcelGen Soil gDNA kit for Illumina sequencing. The quality of the environmental DNA was checked by 0.8% agarose gel electrophoresis and quantified in a Qubit® 2.0 fluorometer. The V3-V4 amplicon libraries were prepared using Nextera XT Index Kit (Illumina Inc.). Primers for the amplification of the V3-V4 hyper-variable regions are described in Supplementary Table S1. The amplicon libraries were purified by 1X AMpureXP beads, checked on an Agilent DNA1000 chip on Bioanalyzer2100 and quantified by Qubit Fluorometer 2.0 using Qubit dsDNA HS Assay kit (Life Technologies).

The Illumina HiSeq paired-end raw reads were checked for quality (base quality, base composition, GC content) using the FastQC tool (Andrews et al., 2010). The QIIME (version: 1.9.1) pipeline (Caporaso et al., 2010) was used to select and cluster the amplicons, followed by taxonomic classification based on the SILVA database. The chimeric sequences were removed from the libraries using the de novo chimera removal method UCHIME implemented in the tool VSEARCH. Only the phototrophic bacterial groups were further analysed and used in this study. All the paired sequencing data have been submitted to the NCBI databases: clone library sequences in GenBank (accession numbers MW671558 to MW671581) and metagenomic sequences in Sequence Read Archive under the BioProject ID: PRJNA703333. The Environmental DNA extraction, PCR amplification were performed at the Indian Institute of Science, Bangalore (India) and sequencing was done on the Illumina HiSeq 2500 platform (Illumina, USA) at Xcelris Labs Limited, Ahmedabad (India).

3.6. 18S metagenomics sequencing

3.6.1. Isolation, qualitative and quantitative analysis of DNA

DNA was isolated from the sample by the XcelGen Soil gDNA kit. The quality of gDNA was checked on 0.8% agarose gel (loaded 5 µl) for the presence of the intact band. The gel was run at 110 V for 30 mins. 1 µl of each sample was loaded in Nanodrop 8000 to determine the $A_{260/280}$ ratio.

3.6.2. Preparation of libraries for 2×250 bp Run Chemistry

The amplicon library was prepared using Nextera XT Index Kit (Illumina Inc.) as per the 18S SSU rRNA gene- Metagenomic Sequencing Library preparation protocol (Part # 15,044,223 Rev. B). Primers 1391f (5′-GTACACACCGCCCGTC-3′) (Lane et al., 1991) and EukBr (5′-TGATCCTTCTGCAGGTTCACCTAC-3′) (Medlin et al., 1988) for the amplification of the V9 variable region of 18S SSU rRNA eukaryotic gene were synthesized in Xcelris PrimeX facility. The amplicon libraries were purified by 1X AMpureXP beads, checked on Agilent DNA1000 chip on Bioanalyzer2100 and quantified by Qubit Fluorometer 2.0 using Qubit dsDNA HS Assay kit (Life Technologies).
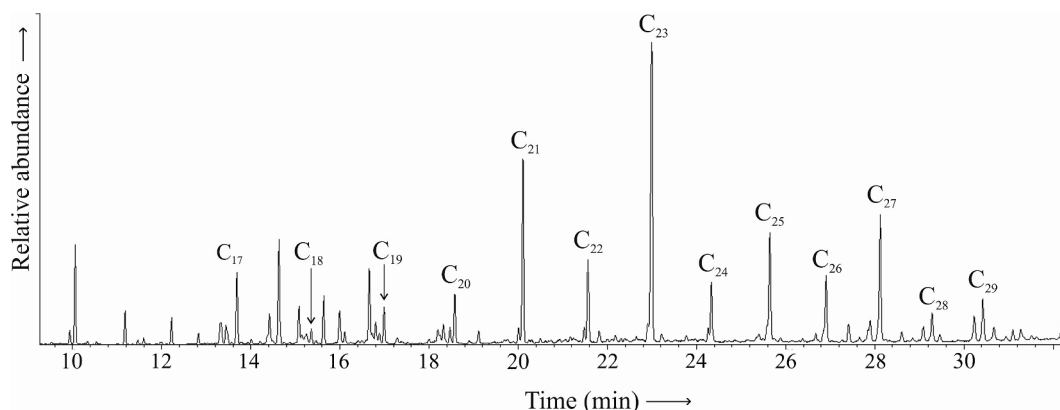

Fig. 2. GC–MS chromatogram of a green benthic mat sample from Lake LH 74 (Discussion Lake).

3.6.3. Cluster generation and sequencing

After obtaining the Qubit concentration for the library and the mean peak size from the Bioanalyzer profile, the library was loaded onto the Illumina platform at an appropriate concentration (10–20 pM) for cluster generation and sequencing. Paired-End sequencing allows the template fragments to be sequenced in both the forward and reverse directions on the Illumina platform. Kit reagents were used to bind samples to complementary adapter oligos on the paired-end flow cell. The adapters were designed based on Maritz et al. (2017) to allow selective cleavage of the forward strands after re-synthesis of the reverse strand during sequencing. The copied reverse strand was then used to sequence from the opposite end of the fragment. The 18S rRNA gene metagenomics sequencing was performed at Xcelris Labs Limited, Ahmedabad (India).

3.7. Microscopic identification

Two to three drops of water samples were put on 22 × 22 mm coverslips and dried for microscopic analysis of the samples. These dried coverslips were then mounted onto permanent glass microscope slides with Canada balsam as a mounting medium. The slides were then studied using an Olympus BX53 compound light microscope, and the photographic documentation was done by the DP26 digital camera attached to the microscope. For several taxa, identification up to species level was not possible due to low preservation and for those organisms where the identity of a taxon could not be determined, were indicated using 'sp.'. A complete list of observed species is provided in Table 2. The microscopic analysis of samples was performed at the Birbal Sahni Institute of Palaeosciences in Lucknow.

Table 2

Molecular characterisation using environmental DNA, taxa identification (family and genus level) and microscopic identification of selected samples from Larsemann Hills.

Sample Type	Location	Molecular Characterization[*]	Taxonomic identification	
			Molecular	Microscopic
Benthic green mat[##]	Lake LH 73, Broknes Peninsula	EUB16S- Negative Cyan16S- Positive Alg18S- Positive *rbcl*- Positive	*Pinnularia* sp. (Diatom, Family: *Pinnulariaceae*) *Bicosoecaceae* *Chromulinaceae* (Algae) *Chrysophyceae* (Algae) *Telonemidae* (Microalgae)	*Pinnularia* sp. (Diatom, Family: *Pinnulariaceae*) *P. australomicrostauron* (Diatom, Family: *Pinnulariaceae*) *Fragillariopsis kerguelensis* (Diatom, Family: *Bacillariaceae*) *Navicula* sp. (Diatom, Family: *Naviculaceae*) *Trichormus* sp. (Cyanobacteria, Family: *Nostocaceae*)
Benthic green mat	Fisher Island	18S Metagenomics	*Chromulinaceae* (Algae) *Chrysophyceae* (Algae) *Ochrophyta*[**]	
Benthic green mat	Meltwater pond, Grovnes Peninsula	EUB16S- Positive Cyan16S- Positive Alg18S- Positive *rbcl*- Positive		*Trichormus* sp. (Cyanobacteria, Family: *Nostocaceae*)
Benthic red-green mat	Lake LH 74, Broknes Peninsula	18S Metagenomics	*Bicosoecaceae* *Xanthophyceae* (Algae) *Chromulinaceae* (Algae) *Chrysophyceae* (Algae) *Bacillariophyceae* (Diatom) *Telonemidae* (Microalgae) *Ochrophyta*[**]	*Pinnularia* sp. (Diatom, Family: *Pinnulariaceae*) *Trichormus* sp. (Cyanobacteria, Family: *Nostocaceae*) Algal spores
Benthic grey mat[#]	Lake LH 35, Eliza Kate Island	18S Metagenomics	*Chromulinaceae* (Algae) *Ochrophyta*[**]	
Green Moss	Fisher Island	18S Metagenomics	*Spumella* sp. (Algae, Family: *Chromulinaceae*) *Chrysophyceae* (Algae) *Ochrophyta*[**]	
Grey moss	Grovnes Peninsula	EUB16S- Negative Cyan16S- Positive Alg18S- Positive *rbcl*- Positive		*Pinnularia borealis* (Diatom, Family: *Pinnulariaceae*) *Chondrocystis* sp. (Cyanobacteria, Family: *Chroococcaceae*) *Gloeocapsa biformis* (Cyanobacteria, Family: *Microcystaceae*) *Oscillatoria* sp. (Cyanobacteria, Family: *Oscillatoriaceae*) Algal spores
Moribund Moss	Fisher Island	18S Metagenomics	*Roseiflexaceae* *Phormidium* sp. (Cyanobacteria) *Chromulinaceae* (Algae) *Telonemidae* (Microalgae) *Chrysophyceae* (Algae) *Ochrophyta*[**]	

[*] Taxonomic and functional gene characterization [EUB16S is Eubacterial 16S rRNA gene, Cyan 16S is Cyanobacterial 16S rRNA gene, Alg18S is Algal 18S rRNA gene and *rbcl* is gene encoding Ribulose-1,5-Bisphosphate Carboxylase]. Further the abundance and phylogeny were supported by 18S metagenomics sequencing.

[**] Taxa identification was possible up to Phylum level (Phylum Ochrophyta).

[##] Samples were collected from a deeper section (3 m) of the lake using a floating platform.

[#] Samples were collected at the shallower depths of the lakes.

3.8. FTIR spectroscopy of moss and benthic mat samples

The FTIR spectroscopic measurements, in the range of 4000–400 cm^{-1}, were recorded using a 3000 Hyperion Microscope with Vertex 80 FTIR System (Bruker, Germany) at SAIF, IIT Bombay. An N$_2$ cooled mercury-cadmium-telluride (MCT) detector was fitted to the FTIR spectrometer. One mg of homogenised powdered sample was mixed with 100 mg of spectroscopic grade KBr powder for spectral measurement. A total of 32 scans were taken for each spectrum. Ten to twelve tonnes of hydraulic pellet pressure were applied to the mixture of powdered organic sample and KBr for 5 min to prepare 1 mm of transparent pellets. The pellets were kept in a sample holder and passed through the IR beam for analysis. The optics of the spectrometer were kept under vacuum, and a continuous flow of purified air was passed through the microscope to avoid absorption bands due to water vapour. After performing background and linear baseline corrections, the spectra were normalised to 1 cm thickness.

4. Results

4.1. Molecular and microscopic identification

Positive PCR amplification of cyanobacterial 16S rRNA genes, universal 18S rRNA and *rbcl* genes were observed in the benthic mats (Table 2). The gene amplification and amplicon size (Vieira et al., 2016), suggest the presence of algal groups such as *Nostocaceae* in the benthic green mat samples (Table 2). Illumina sequencing detected the presence of cyanobacteria and *Chloroflexi* among the phototrophic groups. The benthic green mat shows presence of prokaryotes, especially the bacterial genus *Planococcus* sp., in clone library and Illumina sequencing. Notably, the psychrophilic bacterial genera *Planococcus maitriensis* has been reported from the Schirmacher Oasis in Antarctica (Alam et al., 2003) and *Planococcus stackebrandtii* from the Himalayas (Mayilraj et al., 2005). A high abundance of the cyanobacterial order *Nostocales,* especially the genus *Trichormus* and the phototrophic bacteria *Chloroflexi* (order *Anaerolineales*), possibly thrive in the consortium (Fig. 3).

The 18S SSU rRNA gene-metagenomic sequencing shows that benthic green mats contain several algal families such as *Chrysophyceae*, *Bicosoecaceae*, microalgal family *Telonemidae*, and the diatom genus *Pinnularia* (Table 2). Benthic red-green mats contained the algal family *Xanthophyceae*, along with the previously mentioned algal families that were found in benthic green mats (Table 2). Benthic grey mats also showed the occurrence of the algal family *Chromulinaceae*, and other organisms under the phylum *Ochrophyta* (taxa classification was not possible below phylum level) (Table 2).

Microscopic analysis of the collected samples revealed the presence of four diatom taxa (including species) belonging to three genera, four cyanobacterial taxa (including species) belonging to four genera and algal spores (Fig. 3; Table 2). The benthic mats (Fig. 1) are dominated by diatoms (*Fragillariopsis* sp., *Pinnularia* sp. and *Navicula* sp.) in consortium with *Trichormus* sp. The grey moss shows a diverse assemblage of diatoms (e.g., *Pinnularia borealis*), cyanobacteria (e.g., *Oscillatoria* sp.) and algal resting spores.

4.2. Stable isotope signature of moss and benthic mat consortia

The δ^{13}C values of green (−25.2‰), grey (−23‰), and moribund mosses (−23.8‰ to −23.2‰) are lower than the δ^{13}C values of the green (−16.2‰ to −8.5‰), red-green (−15.6‰ to −8.8‰), red (−14.6‰ to −13.4‰) and grey (−14.4‰ to −12.1‰) benthic mat consortia (Table 3).

Green moss shows the highest δ^{15}N value (19.5‰). The δ^{15}N value is lowest in grey moss (2.8‰). The δ^{15}N values of dry and moribund moss samples range from 8.8‰ to 14.6‰. The green (0.6‰ to 3.8‰), red-green (1.5‰ to 4.6‰), red (1.9‰ to 2.8‰) and grey (−0.6‰ to 7‰) benthic mat consortia show lower δ^{15}N values compared to the mosses.

4.3. Compounds identified by FTIR spectroscopy of moss and benthic mat consortia

The FTIR spectroscopy (spectral range of 4000–400 cm^{-1}) showed distinct absorption peaks at approximately 1030, 1097, 1430, 1650, 2925 and 3450 cm^{-1} in the moss and benthic mat consortia (Figs. 4 and 5). The peaks at 1030 cm^{-1} and 1097 cm^{-1} indicate cellulose and pectin content, respectively (Wagner et al., 2010; Alonso-Simón et al., 2011; Waterman et al., 2018). Peaks at 1430 cm^{-1} indicate benzyl C=C stretches representing phenolic compounds (Waterman et al., 2018). Peaks at 1650 cm^{-1} are assigned to C=O bonds and phenolic ring content in the cells (Alonso-Simón et al., 2011; Waterman et al., 2018). Absorbance peaks at around 2925 cm^{-1} indicate the asymmetric stretching vibrations of CH$_2$ methylene groups of aliphatic chains, especially *n*-alkanes (Lin and Ritz, 1993; Marshall et al., 2005; Sasaki et al., 2009; Shah et al., 2016).

Signals of cellulose (1030 cm^{-1}), phenolic compounds (1430 cm^{-1}), phenolic ring content (1650 cm^{-1}) and aliphatic chains (2925 cm^{-1}) are stronger in grey *B. pseudotriquetrum* compared to green *B. pseudotriquetrum* (Fig. 4).

Compared to green mat consortia, the red-green, red and grey mats show stronger signals of cellulose (1030 cm^{-1}), pectin (1097 cm^{-1}), phenolic compounds (1430 cm^{-1}), phenolic ring content (1650 cm^{-1}) and aliphatic chains (2925 cm^{-1}) (Fig. 5).

4.4. n-Alkane distribution in moss

The *n*-alkane distribution in green, grey and moribund mosses ranges from *n*-C$_{17}$ to *n*-C$_{30}$ (Fig. 6) and shows a strong OEP (1.9–2.8) and near/higher than unity CPI$_{23-31}$ values (1–3.2) (Table 3). The *n*-C$_{21-30}$/*n*-C$_{17-20}$ ratios in green, grey, moribund and dry moribund mosses are 0.3, 0.1, 0.8 and 3.4, respectively. Grey moss shows a relatively higher abundance (88%) of short-chain *n*-alkanes (≤*n*-C$_{20}$) in comparison to the green (69%), moribund (50%) and dry moribund (21%) mosses (Table 3).

4.5. n-Alkane distribution in lake benthic mat samples

Green benthic mat consortia growing in deeper sections (~3 m) of Lake LH 73 in Broknes Peninsula show a higher proportion of long-chain *n*-alkanes (*n*-C$_{23-31}$) with high abundances of *n*-C$_{23}$, *n*-C$_{25}$ and *n*-C$_{27}$ alkanes, and a relatively lower abundance (5%) of short-chain *n*-alkanes (≤*n*-C$_{20}$) with respect to total *n*-alkanes (Table 3). Benthic red-green mat consortia collected from the shallower depths (~30 cm) of Lakes LH A1 and LH 43 on Fisher Island show the highest abundance (29%) of *n*-C$_{23}$ and moderate (20–22%) abundance of short-chain *n*-alkanes with respect to total alkanes present in the samples (Table 3). The relative abundance of short-chain *n*-alkanes is high (46–57%) in the benthic red mat consortia collected from Lakes LH 42 and LH 44 in Fisher Island (Table 3). Benthic grey mat samples collected just below the water level along the fringes of Lake LH 35 in Eliza Kate Island and Lake LH 36 in Grovnes Peninsula show the highest relative abundance (34–71%) of short-chain *n*-alkanes (Table 3). The average *n*-C$_{21-30}$/*n*-C$_{17-20}$ ratios of green, red-green, red and grey mat samples are 8.5, 3.4, 0.9 and 1.1, respectively (Table 3). *n*-Alkanes in the benthic mat consortia range from *n*-C$_{17}$ to *n*-C$_{30}$, and show a strong odd over even predominance (OEP of *n*-C$_{21-25}$) and an above unity carbon preference index (CPI of *n*-C$_{23-31}$) values (Table 3). The OEP does not show any systematic change with the change in colour of the mats, but the CPI$_{23-31}$ shows a gradual increase in values from green/red-green/red (2–4) to grey mat (4–5) samples (Table 3). The gradual increase in CPI$_{23-31}$ values from green to grey mat samples is also shown in Fig. 7. Average Chain Length (ACL) values gradually decrease from green mat consortia (21–25) through red (20–22) to grey mat consortia (18–21.2) (Table 3). This decreasing trend in ACL values is depicted in Fig. 7.

Fig. 3. Commonly occurring diatoms and other algal forms from Larsemann Hills, East Antarctica. (A) *Pinnularia australomicrostauron* (a, b), (B) *Pinnularia* sp. (c, d is girdle view), (C) *Pinnularia australomicrostauron* (e, f is girdle view), (D) *Pinnularia borealis* (g, h), (E) *Fragillariopsis kerguelensis* (i, k), **(F)** algal spore (l, m), **(G)** *Gloeocapsa biformis* (n, o), (H) *Chondrocystis* sp. (p, s), (I) *Oscillatoria* sp. (t, u), (J) *Trichormus* sp. (v, w), (K) algal spore (x).
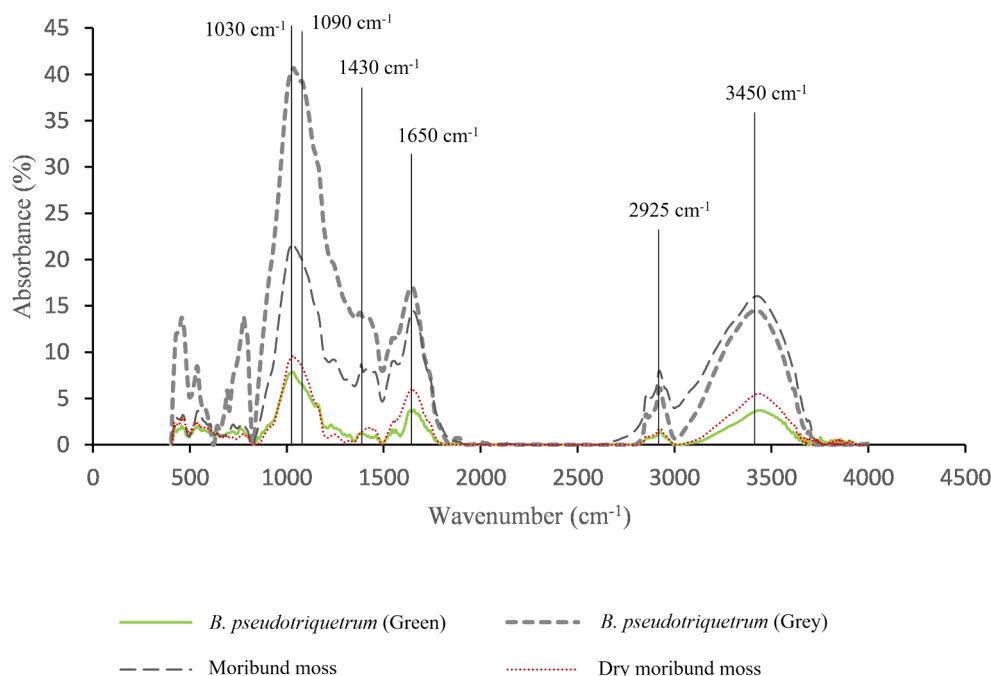
Fig. 4. Averaged FTIR spectra (spectral range of 4000–400 cm^{-1}) of moss samples with distinct absorption peaks of cellulose (1030 cm^{-1}), phenolic compounds (1430 cm^{-1}), phenolic ring content (1650 cm^{-1}) and aliphatic chains (2925 cm^{-1}). These peaks are almost always highest in grey *B. pseudotriquetrum* moss, followed by moribund, dry moribund, and green *B. pseudotriquetrum* moss.
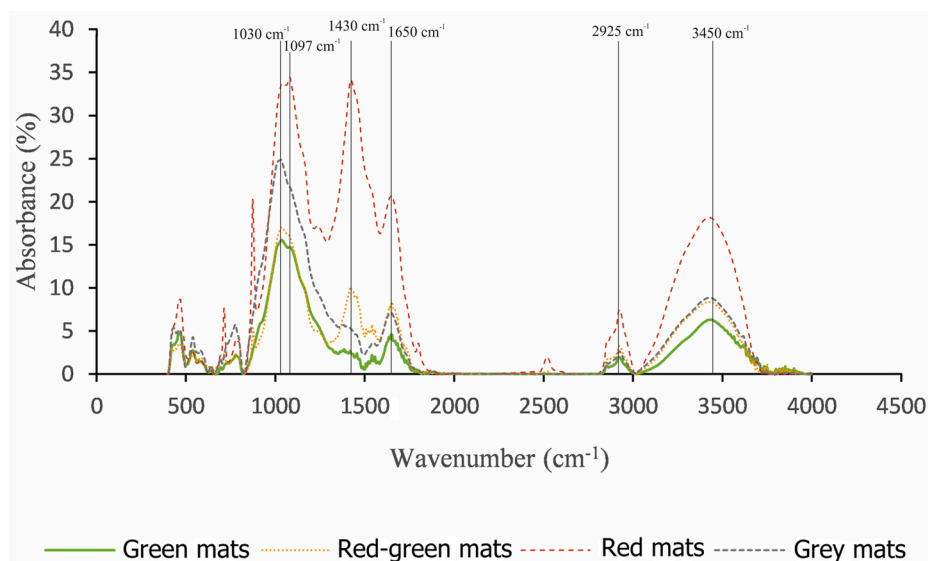

Fig. 5. FTIR spectra (spectral range of 4000–400 cm^{-1}) of the benthic mat samples with distinct absorption peaks of cellulose (1030 cm^{-1}), pectin (1097 cm^{-1}), phenolic compounds (1430 cm^{-1}), phenolic ring content (1650 cm^{-1}) and aliphatic chains (2925 cm^{-1}). Compared to green mat consortia, the red-green, red and grey mats show stronger signals of cellulose (1030 cm^{-1}), pectin (1097 cm^{-1}), phenolic compounds (1430 cm^{-1}), phenolic ring content (1650 cm^{-1}), and aliphatic chains (2925 cm^{-1}).

5. Discussion

5.1. Composition of moss and benthic mat consortia

In the 18S SSU rRNA gene-metagenomic libraries, benthic mat consortia show insignificant variation in their major constituent taxa and are primarily composed of algal families (*Chromulinaceae, Chrysophyceae, Xanthophyceae, Bicosoecaceae*), microalgal family (*Telonemidae*) and diatoms (*Pinnularia* sp.). Environmental DNA and microscopic studies reveal the presence of cyanobacteria, diatoms and algae in moss and lake benthic mat consortia (Table 2).

The δ^{13}C values of green (–25.2‰), grey (–23‰), and moribund mosses (–23.8‰ to –23.2‰) fall within the range of reported δ^{13}C values

of moss (–28‰ to –20‰) in Antarctica (Lee et al., 2009; Strauch et al., 2011; Royles et al., 2016) and Arctic (Skrzypek et al., 2008). The δ^{13}C values (Table 3) of the benthic green mat (–16.2‰ to –8.5‰), red-green mat (–15.6‰ to –8.8‰), red mat (–14.6‰ to –13.4‰) and grey mat (–14.4‰ to –12.1‰) consortia are consistent with δ^{13}C values (–16‰ to –8‰) reported from algal samples of Schirmacher Oasis (Strauch et al., 2011). However, the values are higher than the δ^{13}C values reported for algal organic matter (Dunton, 2001; Lehmann et al., 2002; Gillies et al., 2012). Higher δ^{13}C values of benthic mat consortia may be linked to the alkaline nature (pH > 8) of the lake water where the mats thrive (Table 1). Benthic mat consortia may preferably use HCO$_3^-$ as the source of carbon at high pH conditions (pH ∼ 8 and above). The HCO$_3^-$ is 7‰ to 9‰ higher than the dissolved CO$_2$ (Kaplan and Reinhold, 1999), and the

Table 3

n-Alkane Carbon Preference Index (CPI$_{23-31}$), Odd Over Even Predominance (OEP$_{21-25}$), Average Chain Length (ACL$_{17-31}$), percentage of short-chain n-alkane (n-C$_{17-20}$) content in total n-alkane, long-chain to short-chain n-alkane ratio (n-C$_{21-30}/n$-C$_{17-20}$), Total Organic Carbon (TOC) and stable isotope (δ^{13}C and δ^{15}N) values of the lake benthic mat and moss collected from Larsemann Hills.

Sample Type	Location	[a]CPI$_{23-31}$	[b]OEP$_{21-25}$	[c]ACL$_{17-31}$	C$_{17-20}$/ total alkane (%)	n-C$_{21-30}/n$-C$_{17-20}$	TOC (%)	δ^{13}C (‰)	δ^{15}N (‰)
Lake benthic mats									
Green mat[##]	Lake LH 73, Broknes Peninsula	2.7	3.9	24.2	5	18.1	14.3	–8.5	0.6
Green mat[#]	Lake LH 74, Broknes Peninsula	3.2	4.4	23.2	12	6.2	3.07	–11.7	3.8
Green mat[#]	Lake LH A2, Fisher Island	3.5	7.9	21	46	1.2	1.1	–16.2	3.6
Red–green mat[#]	Lake LH43, Fisher Island	3.4	2.7	22	22	3.1	22.6	–8.8	1.5
Red–green mat[#]	Lake LHA1, Fisher Island	3.6	4.0	22.7	20	3.7	11.8	–15.6	4.6
Red mat[#]	Lake LH 42, Fisher Island	3.8	5.1	20.3	57	0.7	9.97	–13.4	1.9
Red mat[#]	Lake LH44, Fisher Island	3.4	5.9	21.4	46	1.1	15.9	–14.6	2.8
Grey mat[#]	Lake LH35, Eliza Kate Island	4.7	3.1	21.2	34	1.6	8.66	–14.4	5.5
Grey mat[#]	Lake LH35, Eliza Kate Island	3.7	3.3	20.8	40	1.3	9.2	–12.4	7
Grey mat[#]	Lake LH 36, Grovnes Peninsula	4.4	3.3	18.5	71	0.3	10.9	–12.1	–0.6
Mosses									
Bryum pseudotriquetrum (Green)	Fisher Island	2.1	2.6	19	69	0.3	32.3	–25.2	19.5
Bryum pseudotriquetrum (Grey)	Fisher Island	1	1.9	17.9	88	0.1	7.89	–23.0	2.8
Moribund moss	Fisher Island	3.2	2.8	20	50	0.8	24.3	–23.8	14.6
Moribund moss (dry)	Fisher Island	1.9	2.3	23.1	21	3.4	18.5	–23.2	8.8

[a] CPI$_{i-n}$ = 0.5*Σ (X$_i$ + X$_{i+2}$ + … + X$_n$)/ Σ (X$_{i-1}$ + X$_{i+1}$ + … + X$_{n-1}$) + 0.5*Σ (X$_i$ + X$_{i+2}$ + … + X$_n$)/ Σ (X$_{i+1}$ + X$_{i+3}$ + … + X$_{n+1}$), where X is the concentration (van Dongen et al, 2008).

[b] OEP$_{21-25}$ = (C$_{21}$ + C$_{23}$ + C$_{25}$)/(C$_{22}$ + C$_{24}$).

[c] ACL (Average chain length) = Σ (C$_n$ × n)/ Σ (C$_n$), (Bush and McInerney, 2013).

[##] Samples were collected from a deeper section (~3 m) of the lake using a floating platform.

[#] Samples were collected at the shallower depths of the lakes.

fractionation towards the heavier isotopes is higher (up to 11‰) in HCO$_3^-$ under low-temperature conditions (Mook et al., 1974). The process may lead to higher δ^{13}C values (–17‰ to –9‰) in the benthic mat that is comparable to that of C$_4$ plants (O'Leary, 1981; Vuorio et al., 2006).

The δ^{15}N values of green (19.5‰) and grey mosses (2.8‰) fall outside the δ^{15}N signature of *B. pseudotriquetrum* (3.8‰ to 12.2‰), but lie within the range of reported δ^{15}N values of moss-derived organic matter (–9.0‰ to 22.8‰) (Lee et al., 2009). Relatively higher δ^{15}N values of moss samples (2.8‰ to 19.5‰) may suggest assimilation of ^{15}N-enriched nitrogen from penguin guano, which reportedly influences moss isotopic signature in areas near penguin colonies (Wang et al., 2020). The δ^{15}N values in green (0.6‰ to 3.8‰), red-green (1.5‰ to 4.6‰), red (1.9‰ to 2.8‰) and grey (-0.6‰ to 7‰) benthic mat consortia mostly fall within the range of reported δ^{15}N values of algal organic matter (Gillies et al., 2012).

Near-zero δ^{15}N values (Table 3) of green benthic mat consortia from Lake LH 73 (0.6‰) and grey mat consortia from Lake LH 36 (–0.6‰) indicate the presence of atmospheric N$_2$-fixing cyanobacteria (Fogel and Cifuentes, 1993; Talbot and Lærdal, 2000). Higher δ^{15}N values of green benthic mat consortia from Lake LH 74 (3.8‰) and red-green mats from Lake LH A1 (4.6‰) match with the reported δ^{15}N values (1.3‰ to 5.9‰) of red and green algal species collected from the Windmill Islands of Antarctica (Gillies et al., 2012), and indicate a negligible presence of cyanobacteria in these samples. Similarly, the δ^{15}N composition of red benthic mats from Lake LH 42 and LH 44 of Fisher Island (δ^{15}N values 1.9‰ and 2.8‰, respectively) and grey mats collected from Lake LH 35 of Eliza Kate Island (δ^{15}N values 5.5‰ and 7‰, respectively) indicate a negligible cyanobacterial presence. Our study implies that, except in green benthic mat consortia from Lake LH 73 and Lake LH 36, the cyanobacterial population is not significant enough to influence the stable isotope signature of the studied moss and benthic mat samples. The δ^{15}N-based interpretation is consistent with the inference drawn from the microscopic and environmental DNA studies on cyanobacterial presence in the studied samples.

5.2. Colour variation in benthic mats and mosses and its relation to UV-B exposure

We observed darker shades (red and grey) of benthic mats and mosses growing under direct sunlight. Benthic mat consortia at shallower depths are expected to be exposed more to UV-B radiation than those at deeper levels despite the low vertical attenuation coefficients of UV-B in the oligotrophic lakes of the Larsemann Hills (Huovinen et al., 2000; Verleyen et al., 2005). Many researchers have reported an increase in the photoprotective carotenoid with respect to chlorophyll content in Antarctic plants and algae when exposed to UV-B radiation (Newsham, 2003; Robinson et al., 2005). Similarly, Singh et al. (2015) hypothesised that colour change is an adaptive mechanism for preventing the bleaching of chlorophyll molecules under UV radiation. The green *B. pseudotriquetrum* moss is primarily observed in shadow zones, whereas its grey variety and grey-black moribund mosses are mostly found along open meltwater channels that are more exposed to solar radiation. Both cosmopolitan *B. pseudotriquetrum* and endemic *S. antarctici* respond to UV-B exposure by changing leaf colour (Lovelock and Robinson, 2002). *S. antarctici* is least tolerant to UV-B, has lower UV-B screening capability than *B. pseudotriquetrum* and suffers from abnormal morphology and photosynthetic pigment loss when exposed to UV-B (Turnbull and Robinson, 2009). This is reflected in the lower accumulation of UVSC in *S. antarctici* than *B. pseudotriquetrum* (Lovelock and Robinson, 2002). Hence, the observed variation in the benthic mat and moss colour likely reflects the extent of UV-B radiation that the mat and moss consortium receive.
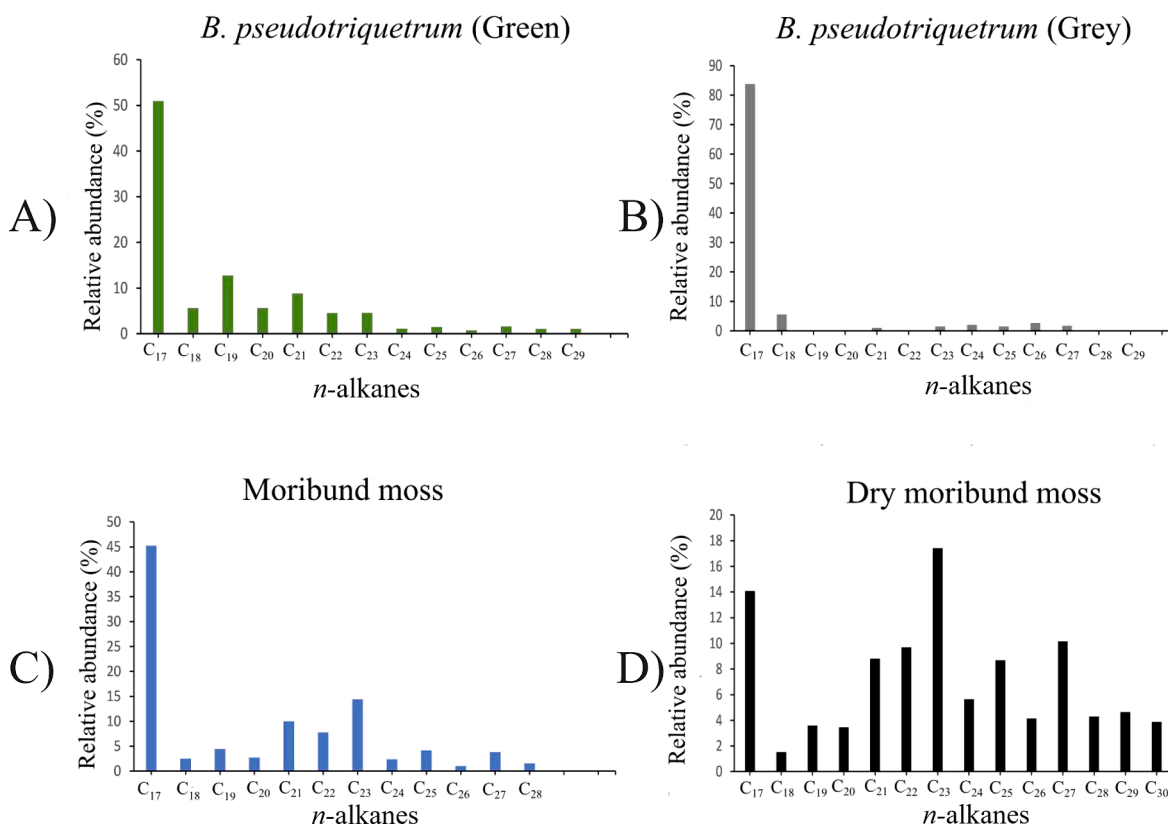
Fig. 6. Normalized relative abundances of *n*-alkanes in: (A) green *B. pseudotriquetrum*, (B) grey *B. pseudotriquetrum*, (C) moribund and (D) dry moribund moss samples. Grey *B. pseudotriquetrum* shows an increased proportion of short-chain *n*-alkanes (*n*-C_{17-20}) compared to green *B. pseudotriquetrum*. Moribund and dry moribund mosses show an increased proportion of long-chain *n*-alkanes (*n*-C_{21-30}) compared to green and grey *B. pseudotriquetrum*.

5.3. Variation in n-alkanes, cellulose, pectin and phenolic compounds in moss and benthic mat consortia and their possible link to UV-B exposure

The FTIR spectroscopic data reveal a higher abundance of cellulose, pectin and phenolic compounds in red and grey benthic mats and mosses, indicating matured cell walls (Waterman et al., 2018). The abundance of phenolic compounds indicates the response of benthic mat and moss to excess UV-B exposure because UV-B induces the production of phenolic compounds using the UV RESISTANT LOCUS 8 (UVR8) pathway (Ballaré et al., 2011; Tilbrook et al., 2013; Singh et al., 2017).

Stronger signals of phenolic rings (1650 cm^{-1}) in the red benthic mat and grey moss indicate higher flavonoid and anthocyanin contents (Figs. 4 and 5) (Waterman et al., 2018). Anthocyanin in grey mosses is known for its role in drought resistance (Chalker-Scott, 1999) and flavonoids are known for their UV absorbing ability (Rozema et al., 2001). The accumulation of cell wall-bound phenolics is attributed to the higher UV tolerance of Antarctic moss species (Clarke and Robinson, 2008). Interestingly, increased absorbance around 2925 cm^{-1} (Fig. 4) indicates a higher *n*-alkane content in grey *B. pseudotriquetrum*. Although the synthesis of *n*-alkanes from phenolic compounds has not been thoroughly studied, the success of such conversion in laboratory experiments suggests the possibility of a similar process in nature (Zhao et al., 2009).

5.4. n-Alkanes in benthic mat consortia and UV-B exposure

The *n*-alkane distribution shows an increase in the abundance of short-chain *n*-alkanes (*n*-C_{17-20}) and a corresponding decrease in the long-chain *n*-alkanes (*n*-C_{21-30}) in red and grey benthic mat consortia growing at shallower depths (Table 3). A relative increase in the short-chain *n*-alkane (*n*-C_{17-20}) content with respect to the total *n*-alkane and

with decreasing sampling depth is observed in the benthic mats (Table 3). The variation in short-chain *n*-alkanes is mirrored by the variation in average chain length (ACL), where lower ACL values are observed in grey mats thriving at the shallower water depth compared to the ACL values of green mats growing at deeper levels (Fig. 7; Table 3). Wang et al. (2018) link the changes in ACL values to temperature. However, temperature variation with depth should be insignificant in Antarctic lakes and should have little influence on the ACL.

The function of *n*-alkanes in benthic mats is not well studied. However, the synthesis of short-chain *n*-alkanes in the epicuticular wax of vascular land plants has been linked to elevated levels of UV-B radiation (Barnes et al., 1996). Similar results were also reported by Tevini and Steinmüller (1987) who studied the effect of increased UV-B radiation in cucumber (*Cucumis sativus* L.) seedlings. A light-dependent conversion of fatty acids (C_{16}–C_{18}) into short-chain *n*-alkanes (*n*-C_{15} to *n*-C_{17}) as a result of the loss of the carboxyl group has also been experimentally demonstrated in microalgae (Sorigué et al., 2016). The possible role of UV-B exposure in the selective production of short-chain *n*-alkanes has rarely been reported in algae (Sorigué et al., 2016). However, such a mechanism, comparable to the UV-B induced *n*-alkane synthesis by vascular land plants, may be followed by Antarctic benthic mat consortia for protection against UV-B radiation.

The relative changes in the *n*-C_{21-30}/*n*-C_{17-20} ratio are closely related to the colour and sampling depth, where an increase in the abundance of short-chain *n*-alkanes (*n*-C_{17-20}) and a corresponding decrease in the abundance of long-chain *n*-alkanes (*n*-C_{21-30}) is observed in benthic mat consortia growing at shallower depths. The increase in the relative abundance of the short-chain *n*-alkanes is likely associated with the increased exposure to UV-B radiation (Huovinen et al., 2000; Verleyen et al., 2005). A higher abundance of phenolic compounds, which is considered a response to excess UV-B exposure (Tilbrook et al., 2013), in
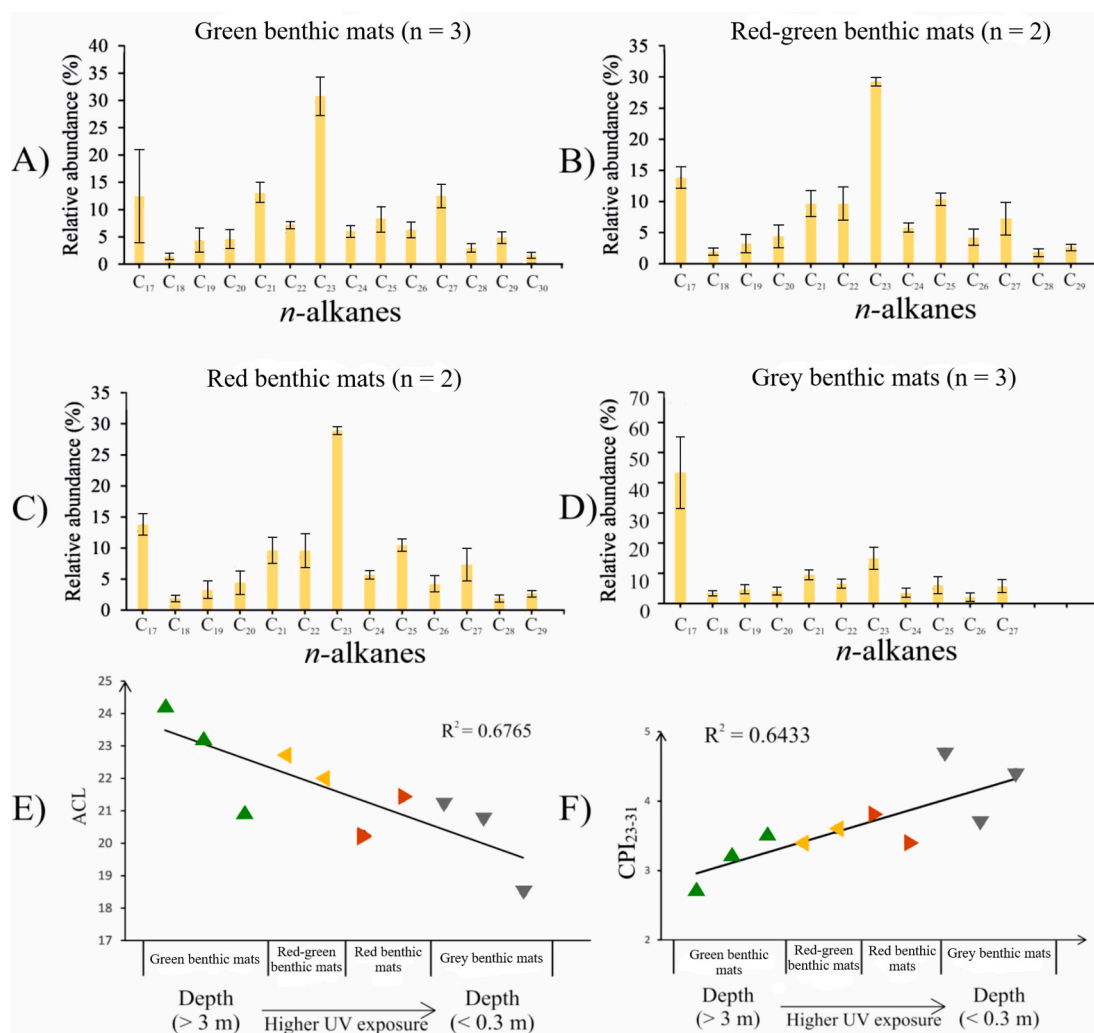
Fig. 7. Normalised average relative abundances of *n*-alkanes in: (A) green (3 samples), (B) red-green (2 samples), (C) red (2 samples), and (D) grey (3 samples) benthic mat samples. The error bars show 1σ standard deviations of the measured relative abundances of *n*-alkanes within mat samples of each group. The graph in the bottom-left (E) shows the decreasing trend of average chain length (ACL) values as one moves from mat consortia growing from deeper (green) to shallower water depths (grey). The graph in the bottom right (F) shows a gradual increase in CPI$_{23\text{-}31}$ values, indicating an increase in the predominance of odd carbon numbered *n*-alkane chains in the benthic mat samples as the sampling water depth decreases.

red and grey benthic mat consortia supports our observation (Fig. 5). The decrease in the long-chain *n*-alkanes (*n*-C$_{21\text{–}30}$) in red and grey benthic mat consortia is associated with a gradual increase in the predominance of odd carbon numbered *n*-alkane chains (evident from the increase in CPI$_{23\text{–}31}$ values) (Fig. 7; Table 3). Notably, the benthic mat samples show higher CPI values (2–5) than CPI values reported in algal samples (~1) (e.g., Zheng et al., 2007). There is a scarcity of published research investigating the link between the synthesis of odd-carbon numbered *n*-alkane and UV-B exposure. Nonetheless, our results suggest that this aspect should be studied further.

5.5. n-Alkane distributions in moss and its link to UV-B exposure and water stress

n-Alkanes are essential components of the extracellular wax of mosses (Haas, 1982), and its synthesis is proposed as a protection mechanism against UV-B (Caldicott and Eglinton, 1976; Kondo et al., 2016). The higher proportion of short-chain *n*-alkanes in grey *B. pseudotriquetrum* than in green *B. pseudotriquetrum* (Table 3) may be linked to the mechanism of *n*-alkane synthesis by vascular land plants. In vascular land plants, enhanced UV-B exposure affects the elongation pathway of acyl chains and causes a shift toward the shorter chain *n*-

alkanes by repressing the synthesis of longer chain *n*-alkanes (Fukuda et al., 2008). Similarly, a higher abundance of short-chain *n*-alkanes in moss may be induced due to enhanced UV-B exposure.

We observed a lesser abundance of short-chain *n*-alkanes in moribund and dry moribund mosses compared to the *n*-alkane distributions in green and grey mosses. The lesser abundance of short-chain *n*-alkanes in moribund and dry moribund mosses might indicate their higher tolerance towards UV exposure than the green mosses (Table 3). On the contrary, a higher abundance of long-chain odd-carbon-numbered *n*-alkanes in moribund and dry moribund mosses (Table 3) is caused by drought stress. This is because the biosynthesis of long-chain *n*-alkanes in extracellular wax, which protects mosses from water stress and plays a role similar to the epicuticular waxes in vascular land plants (Xue et al., 2017), is induced by osmotic stress and is mediated by the gene AtCER1 (Xue et al., 2017). Overexpression of the gene under drought conditions increases the odd over even predominance in *n*-alkanes (Bourdenx et al., 2011). The elongation of fatty acid chains by sequential addition of carbons (C$_2$) leads to decarbonylation and the formation of alkanes in the cuticular wax of non-vascular mosses (Kunst et al., 2005; Shepherd and Wynne Griffiths, 2006). Turnbull et al. (2009) suggest that although the enzymatic repair is inactive in the desiccated state, desiccation results in shrinkage of moss cells, which helps in concentrating the UV

screening compounds, thus decreasing the effects of UV-B damage. The increased proportion of cellulose and pectin in grey *B. pseudotriquetrum* further contributes to the protection against drought stress (Holzinger and Pichrtová, 2016).

5.6. Significance of the findings in the field of paleoenvironment study

Variations in *n*-alkane distributions are widely used in paleoenvironmental and paleoclimate reconstructions (Street et al., 2013; Sawada et al., 2020; Lópéz-Aviles et al., 2021; Seki et al., 2021). However, the influence of UV radiation in the *n*-alkane distribution in organic matter derived from primary producers has not been extensively studied despite its implication in studying geologic intervals with high solar irradiance. Our observation that UV radiation seems to induce short-chain *n*-alkane production in benthic mats and mosses may have implications in paleoenvironmental and paleoclimate interpretations as benthic mats and mosses often constitute a significant portion in aquatic and terrestrial primary production, and contribute a measurable amount of organic matter to sediments. The research outcome has the potential for studying past records of UV irradiance.

6. Conclusions

The studied Antarctic moss and lake benthic mat consortia are characterised by the presence of algae, cyanobacteria and diatoms, but the nitrogen stable isotope signatures reflect a significant presence of cyanobacteria only in green and grey benthic mats from Lake LH 73 and Lake LH 36, respectively. FTIR data indicate the presence of more UV-absorbing compounds in benthic mats growing at shallower depths of lake and mosses growing in exposed areas. The abundance of long-chain *n*-alkanes in moribund and dry moribund mosses reflects water stress, whereas the short-chain *n*-alkanes in green and grey mosses are linked to UV-B exposure. A relatively higher abundance of the short-chain *n*-alkanes compared to long-chain *n*-alkanes in benthic mats growing at the shallower levels of the lakes, along with higher predominance of odd-carbon numbered *n*-alkane chains is likely influenced by UV-B exposure. The research shows the potential of *n*-alkane distributions as a proxy for past changes in UV irradiance where the effects of UV and other environmental changes need to be considered when assessing changes in ACL.

Declaration of Competing Interest

The authors declare that they have no known competing financial interests or personal relationships that could have appeared to influence the work reported in this paper.

Data availability

Data will be made available on request.

Availability of data and material

All the paired sequencing data have been submitted to the NCBI databases- clone library sequences in GenBank (acc. no. MW671558 to MW671581) and metagenomic sequences in Sequence Read Archive (NCBI) under the BioProject ID: PRJNA703333. The rest of the data underlying the study are available from the corresponding author upon reasonable request.

Appendix A. Supplementary data

Supplementary data to this article can be found online at https://doi. org/10.1016/j.orggeochem.2023.104587.

References

Alam, S.I., Singh, L., Dube, S., Reddy, G.S.N., Shivaji, S., 2003. Psychrophilic *Planococcus maitriensis* sp. nov. from Antarctica. Systematic and Applied Microbiology 26, 505–510.

Alonso-Simón, A., García-Angulo, P., Mélida, H., Encina, A., Álvarez, J.M., Acebes, J.L., 2011. The use of FTIR spectroscopy to monitor modifications in plant cell wall architecture caused by cellulose biosynthesis inhibitors. Plant Signalling and Behaviour 6, 1104–1110.

Andrews, S., Gilley, J., Coleman, M.P., 2010. *Difference Tracker*: ImageJ plugins for fully automated analysis of multiple axonal transport parameters. Journal of Neuroscience Methods 193, 281–287.

Ballaré, C.L., Caldwell, M.M., Flint, S.D., Robinson, S.A., Bornman, J.F., 2011. Effects of solar ultraviolet radiation on terrestrial ecosystems. Patterns, mechanisms, and interactions with climate change. Photochemical and Photobiological Sciences 10, 226–241.

Barnes, J.D., Percy, K.E., Paul, N.D., Jones, P., McLaughlin, C.K., Mullineaux, P.M., Creissen, G., Wellburn, A.R., 1996. The influence of UV-B radiation on the physicochemical nature of tobacco (*Nicotiana tabacum* L.) leaf surfaces. Journal of Experimental Botany 47, 99–109.

Bourdenx, B., Bernard, A., Domergue, F., Pascal, S., Léger, A., Roby, D., Pervent, M., Vile, D., Haslam, R.P., Napier, J.A., Lessire, R., Joubès, J., 2011. Overexpression of Arabidopsis *ECERIFERUM1* promotes wax very long-chain alkane biosynthesis and influences plant response to biotic and abiotic stresses. Plant Physiology 156, 29–45.

Caldicott, A.B., Eglinton, G., 1976. Cutin acids from bryophytes: An ω-1 hydroxy alkanoic acid in two liverwort species. Phytochemistry 15, 1139–1143.

Caporaso, J.G., Bittinger, K., Bushman, F.D., DeSantis, T.Z., Andersen, G.L., Knight, R., 2010. PyNAST: a flexible tool for aligning sequences to a template alignment. Bioinformatics 26, 266–267.

Chalker-Scott, L., 1999. Environmental significance of anthocyanins in plant stress responses. Photochemistry and Photobiology 70, 1–9.

Chauhan, A., Bharti, P.K., Goyal, P., Varma, A., Jindal, T., 2015. Psychrophilic *pseudomonas* in Antarctic freshwater lake at Stornes Peninsula, Larsemann Hills over East Antarctica. Springer Plus 4, 582.

Clarke, L.J., Robinson, S.A., 2008. Cell wall-bound ultraviolet-screening compounds explain the high ultraviolet tolerance of the Antarctic moss, *Ceratodon purpureus*. New Phytologist 179, 776–783.

Convey, P., Smith, R.I.L., 2006. Responses of terrestrial Antarctic ecosystems to climate change. Plant Ecology 182, 1–10.

Dunton, K.H., 2001. δ^{15}N and δ^{13}C measurements of Antarctic Peninsula fauna: trophic relationships and assimilation of benthic seaweeds. American Zoologist 41, 99–112.

Ellis-Evans, J.C., Laybourn-Parry, J., Bayliss, P.R., Perriss, S.J., 1998. Physical, chemical and microbial community characteristics of lakes of the Larsemann Hills, Continental Antarctica. Archiv für Hydrobiologie 141, 209–230.

Fogel, M.L., Cifuentes, L.A., 1993. Isotope fractionation during primary production. In: Engel, M.H., Macko, S.A. (Eds.), Organic Geochemistry: Principles and Applications. Plenum, New York, pp. 73–94.

Fukuda, S., Satoh, A., Kasahara, H., Matsuyama, H., Takeuchi, Y., 2008. Effects of ultraviolet-B irradiation on the cuticular wax of cucumber (*Cucumis sativus*) cotyledons. Journal of Plant Research 121, 179–189.

Ghosh, D., Bhadury, P., Routh, J., 2014. Diversity of arsenite oxidising bacterial communities in arsenic-rich deltaic aquifers in West Bengal. India. Frontiers in Microbiology 5, 602.

Gillies, C.L., Stark, J.S., Johnstone, G.J., Smith, S.D., 2012. Carbon flow and trophic structure of an Antarctic coastal benthic community as determined by δ^{13}C and δ^{15}N. Estuarine, Coastal and Shelf Science 97, 44–57.

Gillieson, D., 1990. An atlas of the lakes of the Larsemann Hills, Princess Elizabeth Land, Antarctica (Vol. 74). Australian National Antarctic Research Expeditions, Antarctic Division, Department of the Arts, Sport, the Environment, Tourism, and Territories, Australia.

Green, T.G.A., Kulle, D., Pannewitz, S., Sancho, L.G., Schroeter, B., 2005. UV-A protection in mosses growing in continental Antarctica. Polar Biology 28, 822–827.

Haas, K., 1982. Surface wax of *Andreaea* and *Pogonatum* species. Phytochemistry 21, 657–659.

Hodgson, D.A., Vyverman, W., Sabbe, K., 2001. Limnology and biology of saline lakes in the Rauer Islands, eastern Antarctica. Antarctic Science 13, 255–270.

Hodgson, D.A., Verleyen, E., Sabbe, K., Squier, A.H., Keely, B.J., Leng, M.J., Saunders, K. M., Vyverman, W., 2005. Late Quaternary climate-driven environmental change in the Larsemann Hills, East Antarctica, multi-proxy evidence from a lake sediment core. Quaternary Research 64, 83–99.

Holzinger, A., Pichrtová, M., 2016. Abiotic stress tolerance of charophyte green algae: new challenges for omics techniques. Frontiers in Plant Science 7, 678.

Huovinen, P.S., Penttilä, H., Soimasuo, M.R., 2000. Penetration of UV radiation into Finnish lakes with different characteristics. International Journal of Circumpolar Health 59, 15–21.

Kaplan, A., Reinhold, L., 1999. CO₂ concentrating mechanism in photosynthetic microorganisms. Annual Review of Plant Physiology and Plant Molecular Biology 50, 539–570.

Kondo, S., Hori, K., Sasaki-Sekimoto, Y., Kobayashi, A., Kato, T., Yuno-Ohta, N., Nobusawa, T., Ohtaka, K., Shimojima, M., Ohta, H., 2016. Primitive extracellular lipid components on the surface of the charophytic alga *Klebsormidium flaccidum* and their possible biosynthetic pathways as deduced from the genome sequence. Frontiers in Plant Science 7, 952.

Kunst, L., Samuels, A.L., Jetter, R., 2005. The plant cuticle: formation and structure of epidermal surfaces. In: Murphy, D.J. (Ed.), Plant Lipids. Biology. Utilisation and Manipulation, Blackwell, Oxford, pp. 270–302.

Lane, D.J., 1991. 16S/23S rRNA sequencing. In: Stackebrandt, E., Goodfellow, M. (Eds.), Nucleic Acid Techniques in Bacterial Systematics. John Wiley and Sons, New York, pp. 115–175.

Lee, Y.I., Lim, H.S., Yoon, H.I., 2009. Carbon and nitrogen isotope composition of vegetation on King George Island, maritime Antarctic. Polar Biology 32, 1607–1615.

Lehmann, M.F., Bernasconi, S.M., Barbieri, A., McKenzie, J.A., 2002. Preservation of organic matter and alteration of its carbon and nitrogen isotope composition during simulated and in situ early sedimentary diagenesis. Geochimica et Cosmochimica Acta 66, 3573–3584.

Lin, R., Ritz, G.P., 1993. Studying individual macerals using i.r. microspectrometry, and implications on oil versus gas/condensate proneness and "low-rank" generation. Organic Geochemistry 20, 695–706.

López-Aviles, A., García-Alix, A., Jimenez-Moreno, G., Anderson, R.S., Toney, J.L., Mesa-Fernández, J.M., Jiménez-Espejo, F.J., 2021. Latest Holocene paleoenvironmental and paleoclimate reconstruction from an alpine bog in the Western Mediterranean region: The Borreguil de los Lavaderos de la Reina record (Sierra Nevada). Palaeogeography, Palaeoclimatology, Palaeoecology 573, 110434.

Lovelock, C.E., Robinson, S.A., 2002. Surface reflectance properties of Antarctic moss and their relationship to plant species, pigment composition and photosynthetic function. Plant, Cell & Environment 25, 1239–1250.

Lu, Q.-B., 2022. Observation of large and all-season ozone losses over the tropics. AIP Advances 12, 075006.

Maritz, J.M., Rogers, K.H., Rock, T.M., Liu, N., Joseph, S., Land, K.M., Carlton, J.M., 2017. An 18S rRNA workflow for characterizing protists in sewage, with a focus on zoonotic trichomonads. Microbial Ecology 74, 923–936.

Marshall, C.P., Javaux, E.J., Knoll, A.H., Walter, M.R., 2005. Combined micro-Fourier transform infrared (FTIR) spectroscopy and micro-Raman spectroscopy of Proterozoic acritarchs: a new approach to palaeobiology. Precambrian Research 138, 208–224.

Mayilraj, S., Prasad, G.S., Suresh, K., Saini, H.S., Shivaji, S., Chakrabarti, T., 2005. *Planococcus stackebrandtii* sp. nov., isolated from a cold desert of the Himalayas, India. International Journal of Systematic and Evolutionary Microbiology 55, 91–94.

Medlin, L., Elwood, H.J., Stickel, S., Sogin, M.L., 1988. The characterization of enzymatically amplified eukaryotic 16S-like rRNA-coding regions. Gene 71, 491–499.

Mergelov, N.S., 2014. Soils of wet valleys in the Larsemann Hills and Vestfold Hills oases (Princess Elizabeth land, East Antarctica). Eurasian Soil Science 47, 845–862.

Mook, W.G., Bommerson, J.C., Staverman, W.H., 1974. Carbon isotope fractionation between dissolved bicarbonate and gaseous carbon dioxide. Earth and Planetary Science Letters 22, 169–176.

Newsham, K.K., 2003. UV-B radiation arising from stratospheric ozone depletion influences the pigmentation of the Antarctic moss *Andreaea regularis*. Oecologia 135, 327–331.

O'Leary, M.H., 1981. Carbon isotope fractionation in plants. Phytochemistry 20, 553–567.

Roberts, D., McMinn, A., 1996. Relationships between surface sediment diatom assemblages and water chemistry gradients in saline lakes of the Vestfold Hills, Antarctica. Antarctic Science 8, 331–341.

Robinson, S.A., Wasley, J., Popp, M., Lovelock, C.E., 2000. Desiccation tolerance of three moss species from continental Antarctica. Functional Plant Biology 27, 379–388.

Robinson, S.A., Turnbull, J.D., Lovelock, C.E., 2005. Impact of changes in natural ultraviolet radiation on pigment composition, physiological and morphological characteristics of the Antarctic moss, *Grimmia antarctici*. Global Change Biology 11, 476–489.

Robinson, S.A., Erickson III, D.J., 2015. Not just about sunburn–the ozone hole's profound effect on climate has significant implications for Southern Hemisphere ecosystems. Global Change Biology 21, 515–527.

Robinson, S.A., King, D.H., Bramley-Alves, J., Waterman, M.J., Ashcroft, M.B., Wasley, J., Turnbull, J.D., Miller, R.E., Ryan-Colton, E., Benny, T., 2018. Rapid change in East Antarctic terrestrial vegetation in response to regional drying. Nature Climate Change 8, 879–884.

Royles, J., Amesbury, M.J., Roland, T.P., Jones, G.D., Convey, P., Griffiths, H., Hodgson, D.A., Charman, D.J., 2016. Moss stable isotopes (carbon-13, oxygen-18) and testate amoebae reflect environmental inputs and microclimate along a latitudinal gradient on the Antarctic Peninsula. Oecologia 181, 931–945.

Rozema, J., Broekman, R.A., Blokker, P., Meijkamp, B.B., de Bakker, N., van de Staaij, J., van Beem, A., Ariese, F., Kars, S.M., 2001. UV-B absorbance and UV-B absorbing compounds (*para*-coumaric acid) in pollen and sporopollenin: the perspective to track historic UV-B levels. Journal of Photochemistry and Photobiology B: Biology 62, 108–117.

Sabbe, K., Hodgson, D.A., Verleyen, E., Taton, A., Wilmotte, A., Vanhoutte, K., Vyverman, W., 2004. Salinity, depth and the structure and composition of microbial mats in continental Antarctic lakes. Freshwater Biology 49, 296–319.

Sasaki, K., Inayoshi, N., Tashiro, K., 2009. In situ FTIR-ATR observation of phase transition behavior of *n*-alkane molecules induced by friction motion on a metal interface. The Journal of Physical Chemistry C 113, 3287–3291.

Sawada, K., Ono, M., Nakamura, H., Tareq, S.M., 2020. Reconstruction of Holocene Optimum paleoclimatic variations using long-chain *n*-alkanes and alkenones in sediments from Dabusu Lake, northeastern China. Quaternary International 550, 27–38.

Seki, O., Okazaki, Y., Harada, N., 2021. Assessment of long-chain *n*-alkanes as a paleoclimate proxy in the Bering Sea sediments. Progress in Oceanography 198, 102687.

Shah, Z., Cataluña Veses, R., Silva, R.D., 2016. GC-MS and FTIR analysis of bio-oil obtained from freshwater algae (spirogyra) collected from Freshwater. International Journal of Environmental & Agriculture Research 2, 134–141.

Shepherd, T., Wynne Griffiths, D., 2006. The effects of stress on plant cuticular waxes. New Phytologist 171, 469–499.

Singh, S.M., Pereira, N., Ravindra, R., 2015. Adaptive mechanisms for stress tolerance in Antarctic plants. Current Science 99, 334–340.

Singh, V.P., Singh, S., Prasad, S.M., Parihar, P. (Eds.), 2017. UV-B Radiation: From Environmental Stressor to Regulator of Plant Growth. Wiley Blackwell.

Skrzypek, G., Paul, D., Wojtun, B., 2008. Stable isotope composition of plants and peat from Arctic mire and geothermal area in Iceland. Polish Polar Research 29, 365–376.

Sorigué, D., Légeret, B., Cuiné, S., Morales, P., Mirabella, B., Guédeney, G., Li-Beisson, Y., Jetter, R., Peltier, G., Beisson, F., 2016. Microalgae synthesize hydrocarbons from long-chain fatty acids via a light-dependent pathway. Plant Physiology 171, 2393–2405.

Strauch, G., Haendel, D., Maaß, I., Mühle, K., Runge, A., 2011. Isotope variations of hydrogen, carbon and nitrogen in florae from the Schirmacher Oasis, East Antarctica. Isotopes in Environmental and Health Studies 47, 280–285.

Street, J.H., Anderson, R.S., Rosenbauer, R.J., Paytan, A., 2013. *n*-Alkane evidence for the onset of wetter conditions in the Sierra Nevada, California (USA) at the mid-late Holocene transition, ~ 3.0 ka. Quaternary Research 79, 14–23.

Taberlet, P., Coissac, E., Hajibabaei, M., Rieseberg, L.H., 2012. Environmental DNA. Molecular Ecology 21, 1789–1793.

Talbot, M.R., Lærdal, T., 2000. The Late Pleistocene-Holocene palaeolimnology of Lake Victoria, East Africa, based upon elemental and isotopic analyses of sedimentary organic matter. Journal of Paleolimnology 23, 141–164.

Tevini, M., Steinmüller, D., 1987. Influence of light, UV-B radiation, and herbicides on wax biosynthesis of cucumber seedling. Journal of Plant Physiology 131, 111–121.

Tilbrook, K., Arongaus, A.B., Binkert, M., Heijde, M., Yin, R., Ulm, R., 2013. The UVR8 UV-B photoreceptor: perception, signaling and response. The Arabidopsis book. American Society of Plant Biologists 11.

Turnbull, J.D., Leslie, S.J., Robinson, S.A., 2009. Desiccation protects two Antarctic mosses Aharoni from ultraviolet-B induced DNA damage. Functional Plant Biology 36, 214–221.

Turnbull, J.D., Robinson, S.A., 2009. Accumulation of DNA damage in Antarctic mosses: correlations with ultraviolet-B radiation, temperature and turf water content vary among species. Global Change Biology 15, 319–329.

van Dongen, B.E., Semiletov, I., Weijers, J.W., Gustafsson, Ö., 2008. Contrasting lipid biomarker composition of terrestrial organic matter exported from across the Eurasian Arctic by the five great Russian Arctic rivers. Global Biogeochemical Cycles 22, GB1011.

Verleyen, E., Hodgson, D.A., Sabbe, K., Vyverman, W., 2005. Late Holocene changes in ultraviolet radiation penetration recorded in an East Antarctic lake. Journal of Paleolimnology 34, 191–202.

Vieira, H.H., Bagatini, I.L., Guinart, C.M., Vieira, A.A.H., 2016. *tuf*A gene as molecular marker for freshwater Chlorophyceae. Algae 31, 155–165.

Vuorio, K., Meili, M., Sarvala, J., 2006. Taxon-specific variation in the stable isotopic signatures ($\delta^{13}C$ and $\delta^{15}N$) of lake phytoplankton. Freshwater Biology 51, 807–822.

Wagner, H., Liu, Z., Langner, U., Stehfest, K., Wilhelm, C., 2010. The use of FTIR spectroscopy to assess quantitative changes in the biochemical composition of microalgae. Journal of Biophotonics 3, 557–566.

Wang, J., Axia, E., Xu, Y., Wang, G., Zhou, L., Jia, Y., Chen, Z., Li, J., 2018. Temperature effect on abundance and distribution of leaf wax *n*-alkanes across a temperature gradient along the 400 mm isohyet in China. Organic Geochemistry 120, 31–41.

Wang, X., Liu, X., Fang, Y., Jin, J., Wu, L., Fu, P., Huang, H., Zhang, H., Emslie, S.D., 2020. Application of $\delta^{15}N$ to trace the impact of penguin guano on terrestrial and aquatic nitrogen cycles in Victoria Land, Ross Sea region. Antarctica. Science of the Total Environment 709, 134496.

Wasley, J., Robinson, S.A., Lovelock, C.E., Popp, M., 2006. Climate change manipulations show Antarctic flora is more strongly affected by elevated nutrients than water. Global Change Biology 12, 1800–1812.

Waterman, M.J., Bramley-Alves, J., Miller, R.E., Keller, P.A., Robinson, S.A., 2018. Photoprotection enhanced by red cell wall pigments in three East Antarctic mosses. Biological Research 51, 49.

Wu, W., Ruan, J., Ding, S., Zhao, L., Xu, Y., Yang, H., Ding, W., Pei, Y., 2014. Source and distribution of glycerol dialkyl glycerol tetraethers along lower Yellow River-estuary–coast transect. Marine Chemistry 158, 17–26.

Xue, D., Zhang, X., Lu, X., Chen, G., Chen, Z.H., 2017. Molecular and evolutionary mechanisms of cuticular wax for plant drought tolerance. Frontiers in Plant Science 8, 621.

Zhang, Z., Zhao, M., Yang, X., Wang, S., Jiang, X., Oldfield, F., Eglinton, G., 2004. A hydrocarbon biomarker record for the last 40 kyr of plant input to Lake Heqing, southwestern China. Organic Geochemistry 35, 595–613.

Zhao, C., Kou, Y., Lemonidou, A.A., Li, X., Lercher, J.A., 2009. Highly selective catalytic conversion of phenolic bio-oil to alkanes. Angewandte Chemie International Edition 48, 3987–3990.

Zheng, Y., Zhou, W., Meyers, P.A., Xie, S., 2007. Lipid biomarkers in the Zoigê-Hongyuan peat deposit: Indicators of Holocene climate changes in West China. Organic Geochemistry 38, 1927–1940.